FOI-R--1689-SE
April 2005
ISSN 1650-1942
Technical report

Leif Abrahamsson, Eva Dalberg, Tim Fristedt, Peter Sigray

Measurements and analysis of sound reflected from the seabed

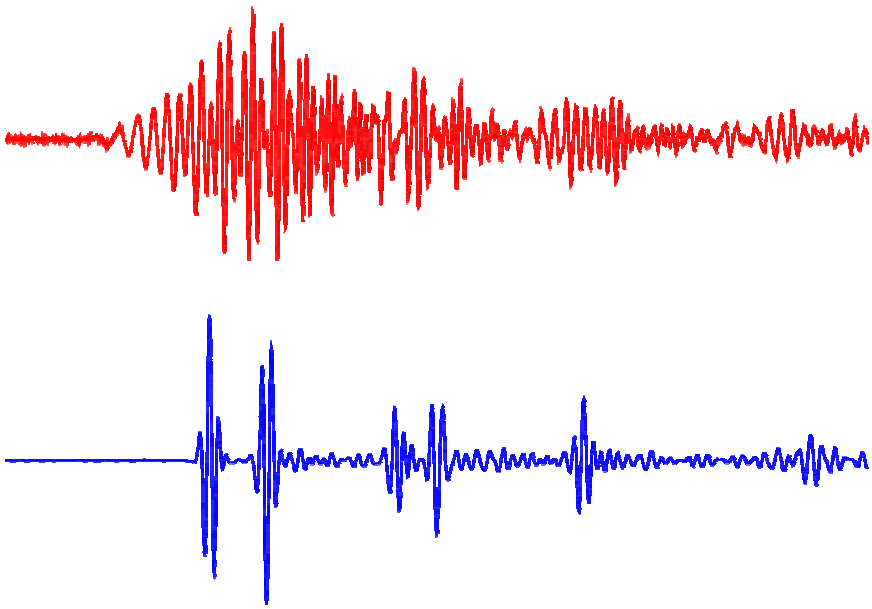

Systems Technology
SE-172 90 Stockholm

SWEDISH DEFENCE RESEARCH AGENCY

Systems Technology
SE-172 90 Stockholm

FOI-R--1689--SE

April 2005

ISSN 1650-1942

Technical report

Leif Abrahamsson, Eva Dalberg, Tim Fristedt, Peter Sigray

Measurements and analysis of sound reflected from the seabed

Issuing organization	Report number, ISRN	Report type
FOI – Swedish Defence Research Agency Systems Technology SE-172 90 Stockholm	FOI-R--1689--SE	Technical report
	Research area code 43 Underwater Sensors	
	Month year April 2005	**Project no.** E60703
	Sub area code 43 Underwater Sensors	
	Sub area code 2	

Author/s (editor/s)	Project manager
Leif Abrahamsson Eva Dalberg Tim Fristedt Peter Sigray	Per Söderberg
	Approved by Monica Dahlén
	Sponsoring agency Swedish Armed Forces
	Scientifically and technically responsible Leif Abrahamsson

Report title

Measurements and analysis of sound reflected from the seabed

Abstract (not more than 200 words)

We present measurements and analysis of acoustic signals which have been reflected by sedimentary layers in the seabed at two sites in the Stockholm archipelago. Reflection data were collected with the transmitter and the hydrophones deployed 5 m above the seafloor and for three offsets in the range 2-60 m. Sediment thicknesses and velocities were determined by travel time analysis according to classical reflection seismics. The analysis shows that the thicknesses of the sediment cover are 18 and 25 m at the two test sites. The speed of sound of the surficial sediment was estimated to 1400 m/s and the density to 1.2-1.3 g/cm^3. The waveforms of the received echoes are highly distorted which indicates that the seabed is locally heterogeneous on a scale of several meters.

In May 2002 a similar experiment was performed in the same area with the transmitter and the hydrophones located on the seafloor. Comparisons between this experiment and the current one with the sonars at some height above the seafloor are made with respect to signal characteristics and inversion results. The conclusion is that both setups work equally well for inversion of reflection data for geoacoustic parameters of the seabed. The measured data are interpreted by means of a ray tracing model for plane-parallel layerings of the sediment. The lack of diffuse scattering of such a model implies that the inversion results must be assessed accordingly.

Keywords

hydroacoustics, geoacoustic parameters, inversion, reflectionseismics, Ricker pulses

Further bibliographic information	Language English
ISSN 1650-1942	**Pages** 30 p.
	Price acc. to pricelist

Utgivare Totalförsvarets Forskningsinstitut - FOI Systemteknik 172 90 Stockholm	**Rapportnummer, ISRN** FOI-R--1689--SE	**Klassificering** Teknisk rapport
	Forskningsområde 4. Ledning, informationsteknink och sensorer	
	Månad, år April 2005	**Projektnummer** E60703
	Delområde 43 Undervattenssensorer	
	Delområde 2	

Författare/redaktör Leif Abrahamsson Eva Dalberg Tim Fristedt Peter Sigray	**Projektledare** Per Söderberg
	Godkänd av Monica Dahlén
	Uppdragsgivare/kundbeteckning Försvarsmakten
	Tekniskt och/eller vetenskapligt ansvarig Leif Abrahamsson

Rapportens titel (i översättning)

Mätningar och analys av ljud som reflekterats från havsbotten

Sammanfattning (högst 200 ord)

I rapporten presenteras mätningar och analys av akustiska signaler som har reflekterats av sedimentskikt i havsbottnar i Stockholms skärgård. Reflektionsdata insamlades med sändare och hydrofoner 5 m ovanför sjöbotten och för tre separationsavstånd i intervallet 2-60 m. Sedimenttjocklekar och ljudhastigheter bestämdes med gångtidsanalys på samma sätt som i klassisk reflektionsseismik. Analysen visar att mäktigheten hos sedimentet är 18 och 25 m på de två mätplatserna. Ljudhastigheten i ytskiktet kan uppskattas till 1400 m/s och densiteten till 1.2-1.3 g/cm^3. Vågformerna hos uppmätta ekon är kraftigt distorderade vilket antyder att sjöbotten är lokalt heterogen på en skala av flera meter. Ett liknande experiment utfördes i maj 2002 med sändare och hydrofoner placerade på sjöbotten. Jämförelser mellan detta experiment och det aktuella med sonarerna några meter ovanför botten presenteras med avseende på signalkarakteristik och inversionsresultat. Slutsatsen är att båda konfigurationerna fungerar i stort sett lika bra för inversion av reflektionsdata för geoakustiska bottenparametrar. Uppmätta signaler analyseras med hjälp av en strålgångsmodell för plana och parallella sedimentskikt. Avsaknaden av diffus spridning i en sådan modell innebär att inversionsresultaten måste bedömas därefter.

Nyckelord

hydroakustik, geoakustiska parametrar, inversion, reflektionsseismik, Rickerpulser

Övriga bibliografiska uppgifter	**Språk** Engelska
ISSN 1650-1942	**Antal sidor:** 30 s.
Distribution enligt missiv	**Pris: Enligt prislista**

Contents

1 Introduction **1**
1.1 Seabed acoustics 1
1.2 The seismic approach 2
1.3 A closely related experiment 2

2 Signal waveforms **2**
2.1 Ricker pulses 3
2.2 FM pulses 4
2.3 Noise considerations 6
2.4 Pulse distortion of the transmitter 7
2.5 The analytic signal 8

3 The field experiment **9**
3.1 The test sites 9
3.2 Experimental configuration 11
3.3 Receiver positions 11
3.4 Source levels 12
3.5 Data acquisition system 13
3.6 Ambient noise 13

4 Signal analysis **14**
4.1 General features of acoustic data 14
4.2 The seabed reflection coefficient 16
4.3 Sub-bottom echoes 20

5 Inversion analysis **21**
5.1 The ray tracing model 21
5.2 The inversion scheme 23
5.3 Inversion results 24

6 Conclusions **27**

7 Future work **27**

1 Introduction

1.1 Seabed acoustics

When a sound wave is generated in a shallow sea it spreads much farther laterally than depthwise because of reflections at the air-sea surface and the bottom. The acoustics around these boundaries is very different from each other. Almost no sound escapes into the air space, while the bottom beneath the seafloor is insonified at varying degrees depending on the angle of incidence and the geoacoustic properties of the bottom. At close range to the transmitter, where the angles of incidence are steep, a great deal of sound is refracted into the seabed. As the incident grazing angles towards the bottom decrease by range from the transmitter, the speed of sound of the surficial sediment is a crucial parameter. If the speed is higher than that of the water (like a sandy bottom), then there is a critical angle of reflection according to Snell's law. It implies that all sound waves with propagation paths at grazing angles below the critical one are trapped in the water column by nearly perfect reflections at the air-sea surface and the bottom. For a muddy bottom the speed of sound may be less than the one in the water. Then there is a reflection loss at each bottom bounce for any angle of incidence. The degree of leakage of sound into the bottom has a profound influence on the sound intensity in the water. Therefore there is a need for methods by which the acoustic properties of the seafloor can be estimated. This report deals with an experiment to determine geoacoustic parameters like speed of sound, density and absorption. The measurements were taken at two locations in Stockholm archipelago in May 2004. Inversion analysis of measured data reveals that the seabed is highly transparent to sound. For example it was found that the speed of sound and the density of the surficial sediment are 1400 m/s and 1.2-1.3 g/cm^3, which means that the impedance contrast with the water is small. The thickness of the sediment overlying a basement of rock was estimated to 18 and 25 m at the two measurement sites.

Geoacoustic parameters like speed of sound, density and absorption must be determined indirectly by interpretation of measured sound pressure levels in the water. Direct measurements from core samples have limitations due to disturbances by the coring operation as well as by postcore handling. Core data provide valuable additional information but not necessarily ground truth. Coring is also too costly for surveying wide areas. A promising alternative is persued in the present work, namely to acquire knowledge of the seabed by inversion of acoustic data. At FOI this research is part of continuing experimental and theoretical studies of inversion techniques for geoacoustic and geoelectric parameters of the seabed [1], [2], [3],[4],[5], [6],[7],[8].

The influence of the seabed on the propagation conditions in the sea has been studied for a long time. Although ever-advanced computational models are used for predictions of underwater sound propagation, the fidelity is limited by uncertainties of input data of bottom parameters. This problem is specifically present in the Baltic Sea, which exhibits a large variability of seabed compositions in limited areas [9], [10]. The need of improving the amount and quality of sediment data was emphasized in a recent studies by Swedish Armed Forces [11] and FOI [12]. It is also desirable to make quantitative estimates of seabed parameters from sonar data under operative conditions (REA - Rapid Environmental Assessment). The strength of the inversion method in this paper

is the computational speed. Pertinent seabed parameters could be extracted from measured data in a few seconds of processing time. The nest step is to apply the inversion scheme on data taken on mobile platforms.

1.2 The seismic approach

The technique being used in this experiment is called reflection seismics or the footprint technique. The basic idea is to probe the seabed by short pulses and to measure the response at a number of receivers at different distances (offsets) from the transmitter. Measured data of arrival times and amplitudes of echoes from sub-bottom interfaces may be converted to thicknesses, velocities, densities and absorption values of layered sedimentary sequences. Applied to shallow sediments this technique is a scaled down version of the classical wide-angle reflection method that has been used in seimic surveying for almost a century. Its power is highlighted by the discovery of gas and oil fields at depths of several kilometers in the earth [13]. Although geophysical techniques based on analysis of time series have evolved over a long time further enhancements are possible. In sediment mappings, one is the use of tow-fish technology for adaptive control of source-receiver depths and offsets. Recent applications of the seismic approach with towed systems are presented in [14], [15]. An overview of geoacoustic inversion techniques of broadband data is given in [16].

1.3 A closely related experiment

In August 2002 a similar experiment was performed at the same test site. In this experiment the source and receivers were put on the seafloor. Bottom deployment improves sound penetration into the seabed and inversion analysis can be based on signals with travel paths solely within the sediment column and thereby eliminating any dependence of the sound velocity profile of the water. The reflection data collected in August 2002 enabled a detailed picture of the sediment cover [17].

In the present experiment a different deployment geometry was applied. Both the transmitter and the receivers were suspended in the water 5 m above the seafloor, as a preparation for future trials on mobile platforms. This paper shows comparisons of measured signals and inversion results from both experiments.

One objective of the present experiment was to see if the inversion results with elevated sensor positions were comparable with those from data received at the bottom. As will be made evident, the overall agreement of the inversion results is good.

2 Signal waveforms

Both the type of acoustic transducer and the probing signals must be adequate for the target of the inversion. This is a wide topic dealing with issues like type of bottom, desired penetration depth, spatial-temporal resolution and source modeling. One particular aspect was formulated as a subproblem, namely to compare the performance of Ricker pulses with frequency modulated (FM) pulses. To that end an FM pulse was designed so that its autocorrelation was identical to the Ricker pulse being used. As a

consequence the matched-filtered receiver output would be identical to the response of the corresponding Ricker pulse in the absence of noise. It implies that the performance in the presence of noise can be assessed by a direct comparison of the matched-filtered time-series.

2.1 Ricker pulses

The original Ricker pulse [18] is defined by

$$r_o(t) = -\frac{2}{\sigma^2}(t^2 - \frac{1}{2}\sigma^2)e^{-\frac{t^2}{\sigma^2}}, \quad t = \text{time } [s], \tag{2.1}$$

which is the second derivative of a Gaussian function. The peak amplitude at $t = 0$ has been normalized to unity. The pulse length, or equivalently the bandwidth, is governed by the parameter σ $[s]$, which is related to the center frequency f_c according to

$$\sigma = \frac{1}{\pi f_c}$$

The Fourier transform of $r_o(t)$ is given by

$$\hat{r_o}(\omega) = \omega^2\sigma^3\frac{\sqrt{\pi}}{2}e^{-\frac{\omega^2\sigma^2}{4}}.$$

The Fourier transform of the autocorrelated Ricker pulse is the square of $\hat{r_o}$, which permits a backtransform in closed form. After normalization to unit peak amplitude, the autocorrelated Ricker pulse is given by

$$r_a(t) = (\frac{1}{3}(\frac{t}{\sigma})^4 - 2(\frac{t}{\sigma})^2 + 1)e^{-\frac{t^2}{2\sigma^2}}. \tag{2.2}$$

The energy, or equivalently the L_2-norm squared, of $r_o(t)$ and $r_a(t)$ are given by

$$\| r_0 \|^2 = \frac{3\sqrt{2}}{8\sqrt{\pi}f_c}, \qquad \| r_a \|^2 = \frac{35}{48\sqrt{\pi}f_c},$$

where f_c is the center frequency of the pulse. The energy of $r_a(t)$ is larger by some 40 percent. Therefore the autocorrelated Ricker pulses were chosen in this experiment.
Three pulses with the center frequencies 0.5, 1 and 2 kHz were used. They are denoted by

$$r_a[.5] \qquad r_a[1] \qquad r_a[2].$$

The 1 kHz pulse $r_a[1]$ and its normalized energy spectrum are plotted in black in Fig. 2.1. It depicts the actual waveform being input to the pulse generator. As can be seen from the graphs, the pulse length T and the bandwidth B are approximately

$$B \approx T^{-1} \approx f_c.$$

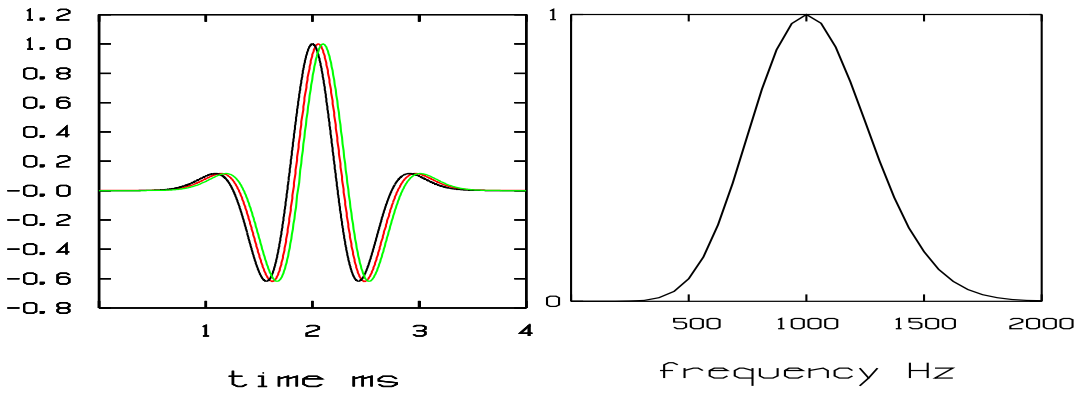

Figure 2.1: *Left: the Ricker pulse* $r_a[1]$ *(black) and the autocorrelated Ricker chirps* $r_c[1, 15]$ *(red) and* $r_c[1, 30]$ *(green). The graphs were slightly displaced to avoid coincident curves. Right: normalized energy spectrum.*

2.2 FM pulses

Linearly frequency modulated (FM) pulses with large time-bandwidth products (BT) are widely used. After pulse compression the time resolution is equal to the inverse of the bandwidth irrespective of the pulse length. This approach improves the signal-to-noise ratio (SNR) by $10 \log (BT)$.

The canonical FM signal is given by

$$f_m(t) = e^{i\gamma t^2}, \tag{2.3}$$

for which the instantaneous frequency is

$$\omega = 2\gamma t.$$

Here γ $[s^{-2}]$ is a positive parameter that controls the sweep rate of frequency, or the bandwidth when f_m is multiplied by an envelope function of compact support. The Fourier transform of $f_m(t)$ is given by

$$\hat{f_m}(\omega) = (\frac{\pi}{\gamma})^{\frac{1}{2}} e^{\frac{i\pi}{4}} e^{-\frac{i\omega^2}{4\gamma}}.$$

The transform

$$\hat{r_c}(\omega) = Ae^{i\omega t_0} e^{\frac{i\omega^2}{4\gamma}} \hat{r_o}(\omega), \quad \omega > 0,$$

with conjugate symmetry for $\omega < 0$, has the design property

$$|\hat{r_c}(\omega)|^2 = |A|^2 \hat{r_a}(\omega).$$

Here A and t_0 are real constants which are chosen such that the inverse $r_c(t)$ has a suitable amplitude and position on the time axis. The new chirp, termed the Ricker chirp and denoted by $r_c(t)$, contains two parameters σ and γ. The bandwidth is set by the parameter σ in the same way as for the Ricker pulse, that is, $\sigma = 1/(\pi f_c)$. The pulse length T is controlled by the parameter γ. T can be chosen freely for pulse

lengths larger than the inverse of the bandwidth. A suitable choice of γ for a given σ and T is given by

$$\gamma = \frac{2}{\sigma T}.$$

We shall use the notation $r_c[f_c, T]$, where f_c $[kHz]$ is the center frequency of the corresponding Ricker pulse and T $[ms]$ is the pulse length. The following Ricker chirps were transmitted in the experiment:

$$r_c[.5, 30] \qquad r_c[1, 15] \qquad r_c[2, 7.5], \tag{2.4}$$

$$r_c[.5, 60] \qquad r_c[1, 30] \qquad r_c[2, 15]. \tag{2.5}$$

The pulses (2.4) and (2.5) are referred to as the short and long Ricker chirps respectively. They are normalized so that the maximum value is unity. The pulses $r_c[1, 15]$ and $r_c[1, 30]$ are depicted Fig. 2.2.

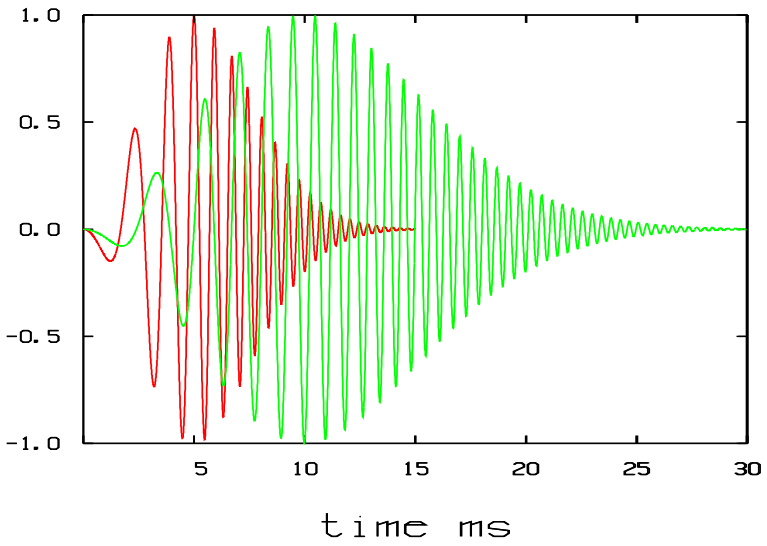

Figure 2.2: *Amplitude modulated FM pulses with the bandwidth 1 kHz and the durations 15 (red) and 30 ms (green). The autocorrelated pulses are shown in Fig. 2.1.*

The autocorrelated pulses, suitably normalized and time shifted, are shown in Fig. 2.1 together with the corresponding Ricker pulse. In order to avoid coincident curves in Fig. 2.1, the compressed chirp signals were slighly displaced for visibility reasons.

The Ricker chirp has a Gaussian-like decay both in the time and the frequency domain. The noise reduction obtained by replica correlation is less than for a conventional chirp with the same time-bandwidth product. On the other hand the matched-filtered Ricker chirp has practically no side-lobes as can be seen from Fig. 2.1.

2.3 Noise considerations

Signal loss due to ambient noise is of main concern in the choice of transmitted waveforms. This issue is now discussed with respect to the signals being used in the experiment.

In the frequency domain the received pressure $p_a(t)$ using a Ricker source pulse $r_a(t)$ is given by

$$\hat{p_a}(\omega) = H(\omega)\hat{r_a}(\omega) + \hat{n}(\omega),$$

where H is the transfer function, or the impulse response, for wave propagation between the source and the receiver. The ambient noise $\hat{n}(\omega)$ is assumed to be white with statistics

$$E\{\hat{n}(\omega)\} = 0 \quad \text{and} \quad E\{\hat{n}^2\} = n_0^2,$$

where n_0 is the one-sided spectral density $[\mu Pa/H^{\frac{1}{2}}]$. In the time domain the expectation of the pressure square can be written as

$$p_a^2(t) = p^2(t) + \int_{B_L}^{B_R} n^2(f)df,$$

where $p(t)$ is the noise-free signal. Here it is assumed that a bandpass filter with a rectangular response over the bandwidth

$$B = B_R - B_L,$$

has been applied. If the spectral density is constant, then for a peak amplitude P of p_a, SNR is given by

$$SNR = 10log\frac{P^2}{n_0^2 B} \quad [dB]. \tag{2.6}$$

Consequently, as the bandwidth increases SNR is degraded by $10logB$, which could be severe for Ricker pulses in noisy environments.

If the propagating medium is stationary, noise reduction can be achieved by emitting a sequence of pulses which are coherently summed at the receiver. If M pulses are used, SNR is improved by $10logM$ [19].

Turning to the Ricker chirp $r_c(t)$, we have

$$\hat{p_c}(\omega) = H(\omega)\hat{r_c}(\omega) + \hat{n}(\omega).$$

Correlation of the received pressure $p_c(t)$ with $r_c/||r_c||^2$ implies

$$\frac{1}{||r_c||^2}\bar{\hat{r}}_c(\omega)\hat{p}_c(\omega) = \frac{1}{||r_c||^2}(\bar{\hat{r}}_c(\omega)H(\omega)\hat{r}_c(\omega)) + \frac{\bar{\hat{r}}_c(\omega)\hat{n}(\omega)}{||r_c||^2}. \tag{2.7}$$

Now according to the design criterion of r_c

$$\hat{r}_a(\omega) = \frac{|\hat{r}_c(\omega)|^2}{||r_c||^2},$$

which implies that the matched-filtered output (2.7) is the same as the response of the corresponding Ricker pulse in the absence of noise. In the time domain the expectation of the pressure squared of the matched-filtered signal is given by

$$p_m^2(t) = p^2(t) + \frac{1}{||r_c||^4} \int_{B_L}^{B_R} |\hat{r}_c(f)|^2 \hat{n}^2(f) df.$$

For a constant noise spectrum n_0^2 the noise term is given by

$$\frac{1}{||r_c||^4} \int_{B_L}^{B_R} |\hat{r}_c(f)|^2 \hat{n}^2(f) df \approx \frac{n_0^2}{||r_c||^2},$$

leading to the SNR

$$SNR = 10 \log \frac{P^2 ||r_c||^2}{n_0^2}.$$

The gain as compared with the SNR (2.6) of the Ricker pulse is

$$\text{Gain} = 10 \log B ||r_c||^2.$$

When $r_c(t)$ has a rectangular envelope with unit amplitude, then $||r_c||^2$ is approximately equal to the pulse length T. In this case the gain is $10 log BT$. For the Ricker chirp with a Gaussian-like envelope the gain is reduced by some 8 dB as compared to a rectangular chirp of the same duration. The short and long Ricker chirps (2.4) and (2.5) have $BT = 15$ and $BT = 30$ with the gains 4 and 7 dB respectively. There are many references on matched filtering [20],[19].

2.4 Pulse distortion of the transmitter

The frequency dependence of the power output of the receiver amounts to 10 dB per octave within the frequency range of interest, see Sec. 3.4. It corresponds to an amplitude modulation

$$A = (\frac{f}{f_c})^{\frac{1}{2 \log 2}} \approx (\frac{f}{f_c})^{1.66},$$

where f_c is the center frequency of the pulse. It has an appreciable effect on the generated waveform as can be seen in Fig. 2.3 for $f_c = 1$ kHz. It can be shown analytically that the center frequencies 0.5, 1 and 2 kHz of the Ricker pulses are shifted to 594, 1190 and 2380 Hz. Waveforms predicted by the above model agree well with measured ones.

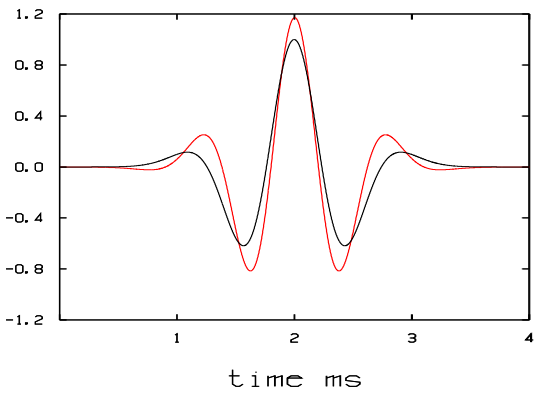

Figure 2.3: *The 1 kHz Ricker pulse* $r_a[1]$ *(black) and the predicted waveform generated by the source (red).*

2.5 The analytic signal

The received pressure $p_r(t)$ is a real field quantity. The complex pressure $p_c(t)$ is defined by

$$p_c(t) = p_r(t) + ip_i(t),$$

where $p_i(t)$ is the Hilbert transform of $p_r(t)$, that is,

$$p_i(t) = H[p_r(t)] = \frac{1}{\pi}\int_{-\infty}^{\infty}\frac{p_r(\tau)}{\tau - t}d\tau.$$

In practice $p_c(t)$ is found by an inverse Fourier transform over positive frequencies according to

$$p_c(t) = \frac{1}{\pi}\int_0^{\infty}\hat{p}_r(\omega)e^{-i\omega t}d\omega,$$

where $\hat{p}_r$ is the Fourier transform

$$\hat{p}_r(\omega) = \int_{-\infty}^{\infty}p_r(t)e^{i\omega t}dt, \quad \omega > 0.$$

Alternatively, $p_i(t)$ can be obtained by setting

$$\hat{p}_i(\omega) = -i\hat{p}_r(\omega), \quad \omega > 0,$$

with complex conjugation for $\omega < 0$. The transforms are implemented numerically by FFT.

The envelope squared of the real signal is defined by

$$|p_c(t)|^2 = p_r^2(t) + p_i^2(t).$$

In this paper the signal level of the measured pressure amplitude $p_r(t)$ is expressed as

$$10\log|p_c(t)|^2 \quad [dB],$$

and transmission loss (TL) is obtained by subtracting the signal level from the source level.

The 1 kHz Ricker pulse $r_a[1]$, its Hilbert transform and the envelope squared are displayed in Fig. 2.4.

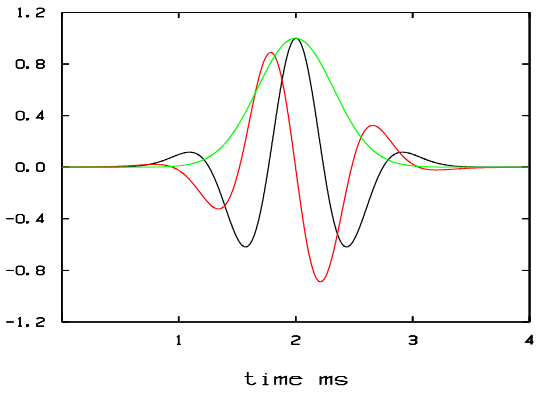

Figure 2.4: *The 1 kHz Ricker pulse* $r_a[1]$ *(black), the Hilbert transform (red) and the envelope squared (green).*

3 The field experiment

3.1 The test sites

The measurements were taken at two sites in Horsfjärden in the Stockholm archipelago on May 12 and 13, 2004. These sites are referred to as N04 and S04, while those in August 2002 experiment are denoted by N02 and S02, see Fig. 3.1.

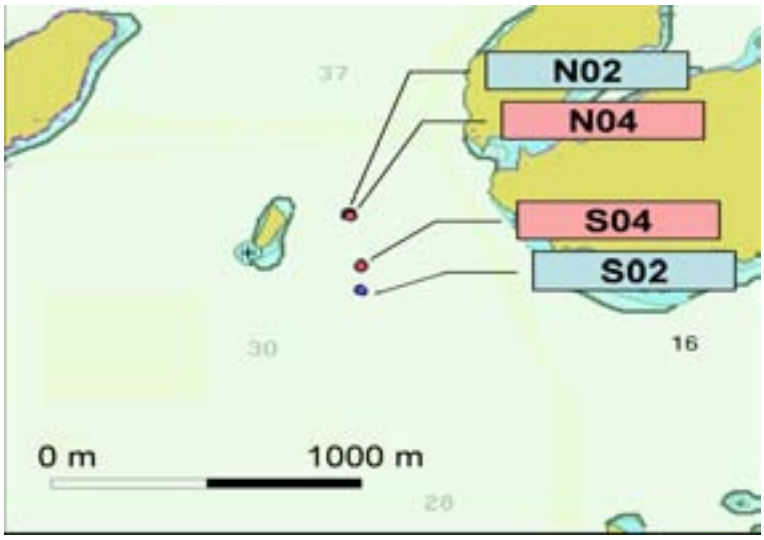

Figure 3.1: *An overview of the measurement area with the sites N04 and S04 in May 2004 and N02 and S02 in August 2002.*

The GPS coordinates of the transmitter positions from north to south are listed in Tab. 3.1.

The two northern sites N02 and N04 are virtually at the same location. The positions of S04 and S02 are to the south of N02 and N04 by some 250 m. The separation distance between S04 and S02 is 72 m.

The water depths at N04 and S04 are around 22 and 18 m respectively with variations

site	latitude N	longitude E
N02	59° 02.83	18° 07.62
N04	59° 02.829	18° 07.632
S04	59° 02.699	18° 07.670
S02	59° 02.66	18° 07.67

Table 3.1: Transmitter positions in GPS coordinates.

within ± 1 m over the range spanned by the positions of the source and receivers.

A description of the geology of the area around the test site is presented in [10], [21]. In general the crystalline bedrock is overlain by unconsolidated sediments of different types like till, glacial and postglacial clays and mud. Vertical profiling by bottom penetrating sonars and reflection seismics show that this structure is very irregular [21]. The depth to the bedrock exhibits large variations which are partly smoothed by pockets of sediments. The thickness of the sediment cover at N02 was estimated to 18 m [17]. It is expected to grow southwards. The surface roughness and impedance was estimated in [22] using echo data from a parametric sonar. It was found that the seafloor has a small-scale roughness of the order of a few centimeters. The impedance was estimated to $1.6 \cdot 10^6 \quad [kg/m^2 s]$, which indicates that the surficial sediment is very soft. Several reverberation measurements in the frequency range 2-20 kHz have been conducted in the area. They show that the backscattering strength is some 10 dB larger than expected from this type sediment. On the other hand the reverberation decays rapidly with neglible contributions beyond some 250 m. One reason for this is the small footprint of the parametric sonar, another is that seabed volume reverberation is strong compared with surface scattering [10], [23], [24].

Sound velocity profiles were measured at the time of the acoustic recordings in the afternoon on May 12 and 13, 2004. They are shown in Fig. 3.2 together with the profile at N02 from August 2002.

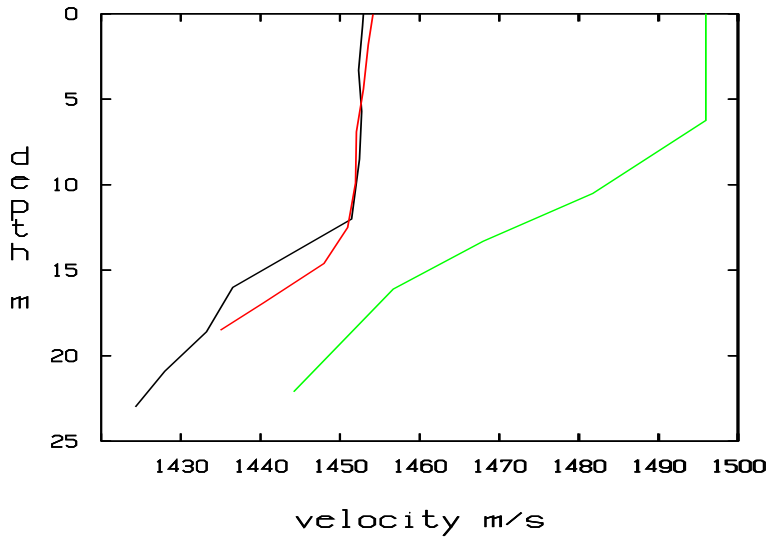

Figure 3.2: *The sound speed profiles at N04 (black), S04 (red) and N02 (green).*

3.2 Experimental configuration

Three hydrophones and one transmitter were used. They were submerged 5 m above the seafloor using ropes connected to anchors and buoys. The offset between the transmitter and the first hydrophone was 2 m. This distance was ensured by tethering to a iron rod mounted horizontally on a square concrete block of sufficient weight for bottom mooring. Hydrophones two and three were deployed at the nominal offsets 25 and 50 m (measured by a rope from the support ship Skotten). The deployment geometry is shown in Fig. 3.3. The data acquisition system was placed aboard Skotten.

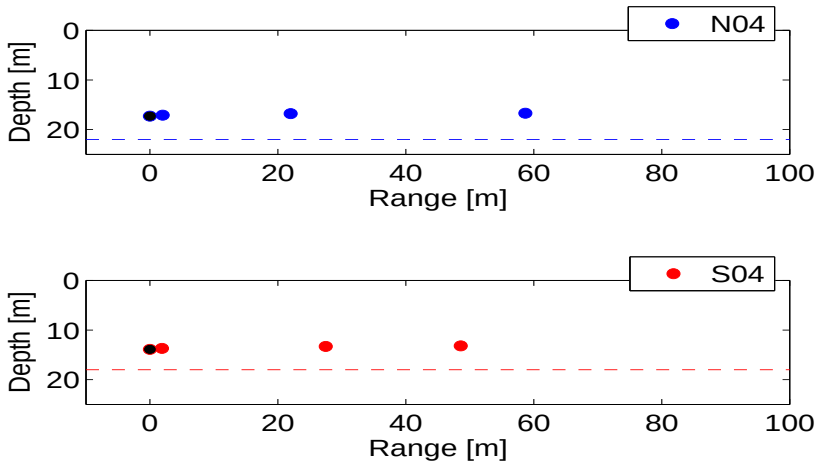

Figure 3.3: *A schematic of the deployment geometry at the two test sites N04 and S04.*

3.3 Receiver positions

Fig. 3.4 shows measured signals at the receivers that were deployed some 25 m from the source positions at N04 and S04. The source pulse is the 2 kHz Ricker pulse.

The direct arrival and the surface reflection are the most conspicuous features at the beginning of the recording. They are also easily identified by computer analysis using amplitude, energy or correlation detectors. Although these arrivals do not carry information of bottom parameters, they are useful for the determination of the positions and the power output of the source.

Two approaches were tested for precise acoustic localization of the receivers. As the depth position was known, the range can be obtained by multiplying the travel time with the mean velocity at the depths of the source and the receiver. Although temporal resolution improves by the frequency, it was found that the distances obtained using 0.5, 1 and 2 kHz Ricker pulses were consistent within ± 0.2 m.

An alternative approach is to use both the direct and the surface reflected arrivals for determination of both range and depth. In case of isovelocity the range-depth position is simply obtained as an intersection point of two circles with the origins at the source position and its mirror point with respect to the sea surface, and with radii determined by measured travel times. This approach was extended by ray tracing to account for

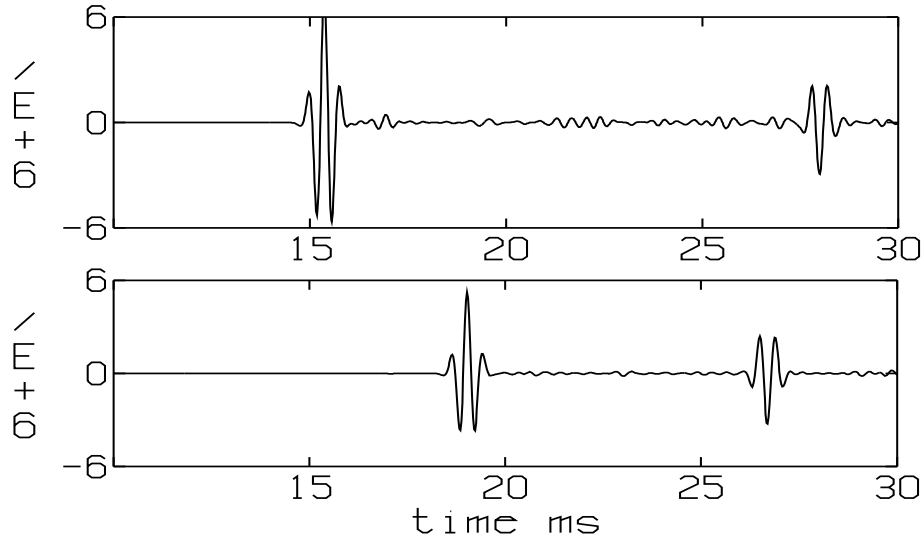

Figure 3.4: *Measured pressure amplitudes* [μPa] *at N04-R2 (top) and S04-R2 (bottom).*

sound velocity variations by depth. The range-depth positions obtained in this way agreed within ±1 m with those determined by direct arrivals only and prescribed depth positions. The cause of the departure is due to uncertainties of the bottom depths at source and receiver positions rather than imprecise data of travel times. In conclusion, the relative range-depth position can be determined using a single source, provided that the direct and surface reflected arrivals are well separated.

The result of the position analysis is presented in Tab. 3.2, where the receivers are denoted by R1, R2 and R3. The bottom-located receiver positions at N02 and S02 have also been included for later reference. At S02 data were collected only at two pairs of source-receiver positions one of which (R2) having the source at the depth 14.1 m or 4.2 m above the seafloor.

test	R1		R2		R3		source	water
site	range	depth	range	depth	range	depth	depth	depth
N02	13.4	22.5	22.9	22.5	45.0	22.5	22.5	22.5
N04	2.0	17.1	22.0	16.8	58.7	16.7	17.3	21.9
S04	1.9	13.7	27.5	13.3	48.6	13.2	13.9	18.5
S02	10.8	18.3	17.9	18.3	-	-	18.3 (14.1)	18.3

Table 3.2: *The geometry of the receivers, the depth of the source and the water depth.*

3.4 Source levels

Even though the power output of the transmitter is known, a field calibration provides a check on deviations due to the drive voltage or the environment. Once the relative source-receiver positions have been determined as described above, the source level can be obtained using the direct or the surface reflected arrivals relying on the calibration of the hydrophones. The source level is obtained by subtracting the geometric loss of propagation from the measured intensity. The results of applying this approach on

all signals, any receiver or any propagation path, were consistent within ±1 dB. The source levels were found to be 139, 149 and 160 [dB re 1 μPa] for 0.5, 1 and 2 kHz respectively.

3.5 Data acquisition system

The receivers had a sensitivity of -170 dB re 1 V/μPa including 14 dB pre-amplification from 2 Hz up to at least 10 kHz. A further gain of 20 dB was used for the hydrophone nearest the source, while a gain of 40 dB was used for the other two receivers. The signals were recorded using a 16 bit analogue-to-digital converter using a sampling frequency of 50 kHz. To increase the signal-to-noise ratio the response from 50 or 200 pulses were stacked before storage on disc.

3.6 Ambient noise

Ambient noise was measured at both sites on May 12 and 13 2004. The wind speed was 5-6 m/s and there was no ship traffic in the near vicinity of the experiment site. There were no significant differences of the noise levels neither at the two sites nor at the receivers. The left picture in Fig. 3.5 shows the noise spectrum level at S04-R2 for the cases with and without stacking. The stacked noise curve is an average of 100 recordings each comprising a time interval of 250 ms. This measurement was performed in the same way as if a sequence of 100 pulses had been transmitted followed by a coherent addition of the response. The expected gain of such an averaging is 20 dB which agrees well with the lower level of the stacked noise measurement in Fig. 3.5.

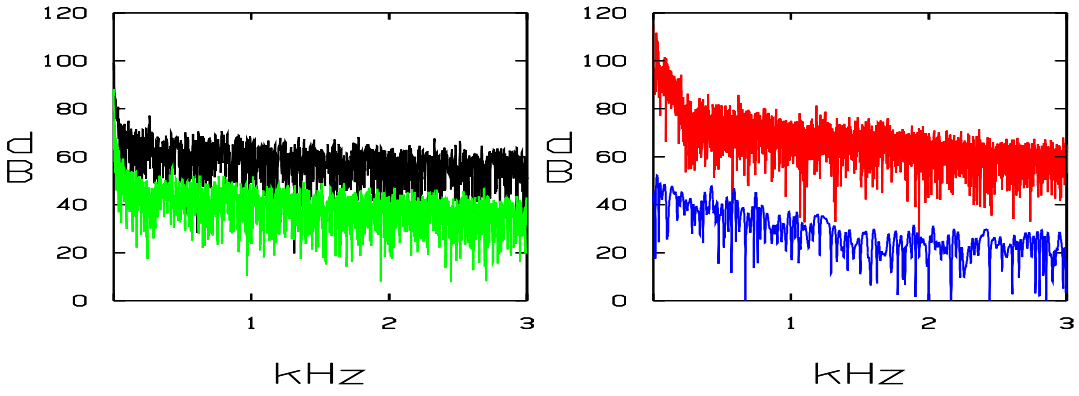

Figure 3.5: *Left: The spectral noise level* [dB *re 1* $\mu Pa/\sqrt{Hz}$] *at S04-R2 for unstacked (black) and stacked (green) recordings. Right: noise measurments (unstacked) taken in the vicinity of Landsort in May 2002 (red) and in Horsfjärden on May 10 2004 (blue).*

For comparison noise spectrum levels measured at two other locations are shown to the right in Fig. 3.5. One of these was taken on May 10 at a nearby site at the wind speed 9-10 m/s. The noise level is exceptionally low.

The noise level represented by the red curve in Fig. 3.5 was measured during the BAROC trial in May 2002 [25]. The recordings were made in the vicinity of Landort in an area of varying bathymetry with an average water depth of 90 m. Transmission loss

measurements taken over 30 km showed that the propagation conditions were excellent. This is explained by the presence of an underwater sound channel in the water with its axis at the depth 60 m. The noise level is high despite moderate winds (4-5 m/s) even at frequencies where the ship noise is less significant.

4 Signal analysis

4.1 General features of acoustic data

Some typical features of the measured time traces during early and late time-windows are displayed in Fig. 4.1 and 4.2. At the beginning of the recording we see a number of distinct arrivals in Fig. 4.1. Around 40 ms after the first arrival the echoes become less discernable as they are mixed up with a train of pulses. The signals in Fig. 4.2 display a noise-like behavior which presumably consists of multipath contributions from many scatterers within an area which expands by time (reverberation).

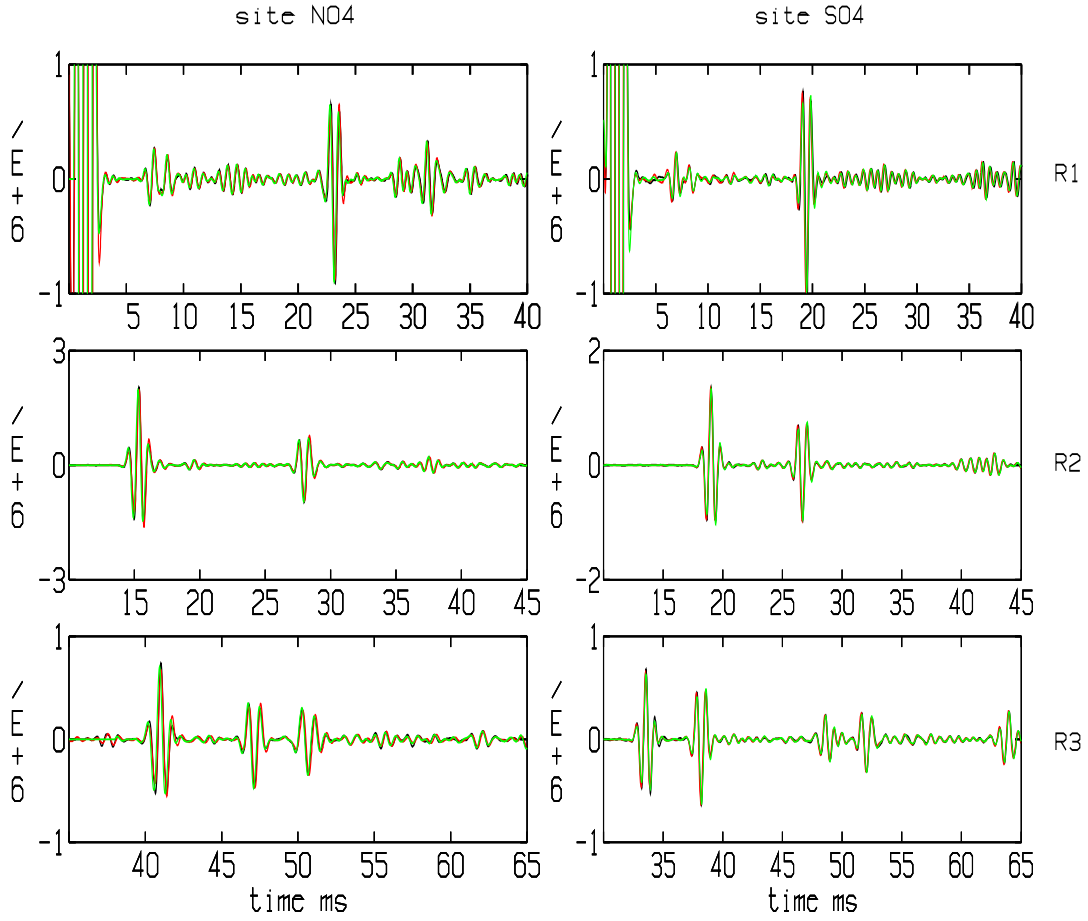

Figure 4.1: *The early part of the measured time traces of pressure* $[\mu Pa]$ *at N04 (left) and S04 (right) at the receivers R1, R2 and R3 (top to bottom). Three curves are depicted in each panel corresponding to the 1 kHz source pulses* $r_a[1]$ *(black),* $r_c[1, 15]$ *(red) and* $r_c[1, 30]$ *(green). The matched-filtered output of the Ricker chirps are nearly identical to the response of the Ricker pulse.*

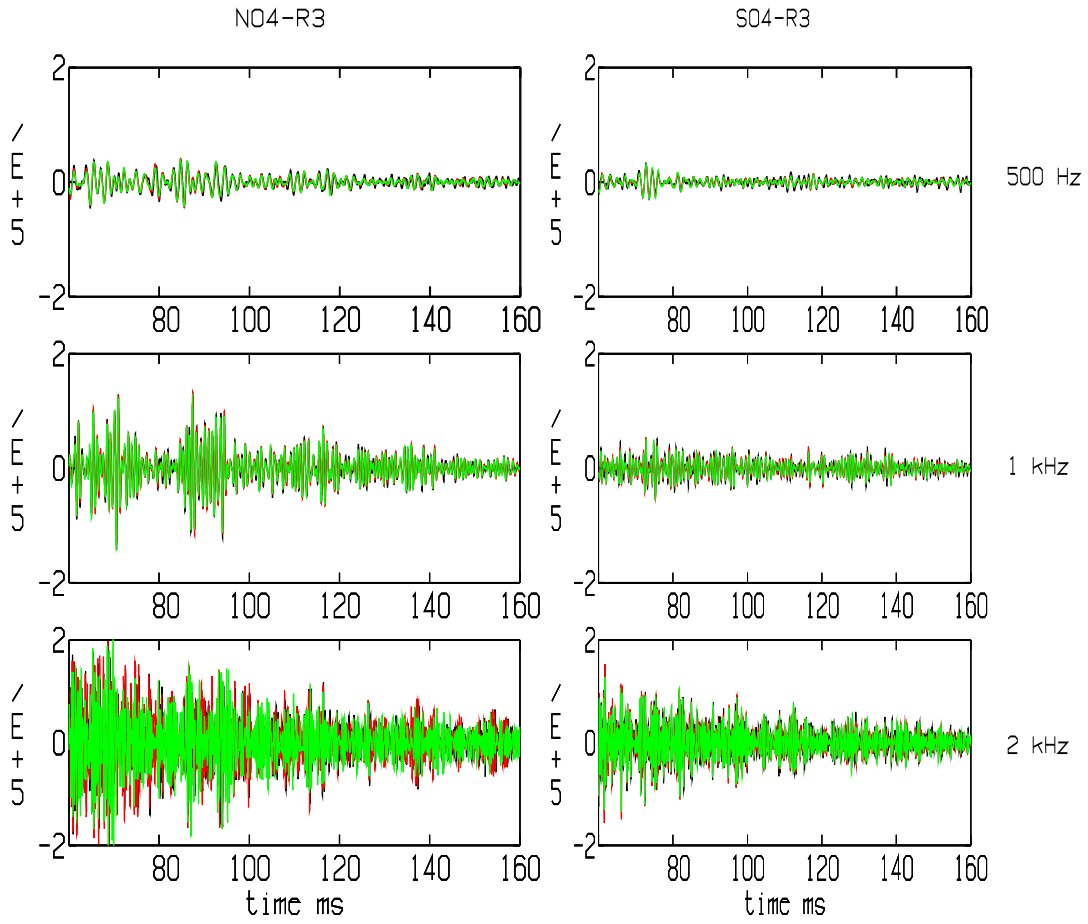

Figure 4.2: *The the measured time traces of pressure* $[\mu Pa]$ *at N04-R3 (left) and S04-R3 (right) in the time-window 60-160 ms. The panels from top to bottom display responses of source pulses centred at 0.5, 1 and 2 kHz. Each panel contains three curves corresponding to the Ricker pulse (black), the short and long matched-filtered Ricker chirps (red and green).*

In each panel in Fig. 4.1 and 4.2 three traces are depicted corresponding to three different source pulses, the Ricker pulse (black) and the short and long Ricker chirps (red and green). An example of the measured response of a Ricker chirp and its matched-filtered output is displayed on the front cover of this paper. The signal is $r_c[1, 30]$ at S04-R3, which is also shown at the lower right panel in Fig. 4.1.

At the head of the time series the response of the Ricker pulse is nearly identical to those of the matched-filtered outputs of the Ricker chirps. The reason for this is that the SNR is at least 25 dB. Fig. 4.3 shows averaged signal levels taken over a left-adjusted sliding window of 20, 10 and 5 ms for the long Ricker chirps centred at 0.5, 1 and 2 kHz, respectively. The corresponding noise levels are shown at the bottom of Fig.4.3.

The expected gain of stacking and correlation is 20 and 7 dB, respectively. The noise reduction of the stacked data is so effective that the additional gain of match-filtering is insignificant. The same remark applies to the tail of the signal displayed in the top and middle frames of Fig. 4.2. The traces of the lower panels of Fig. 4.2 exhibit some

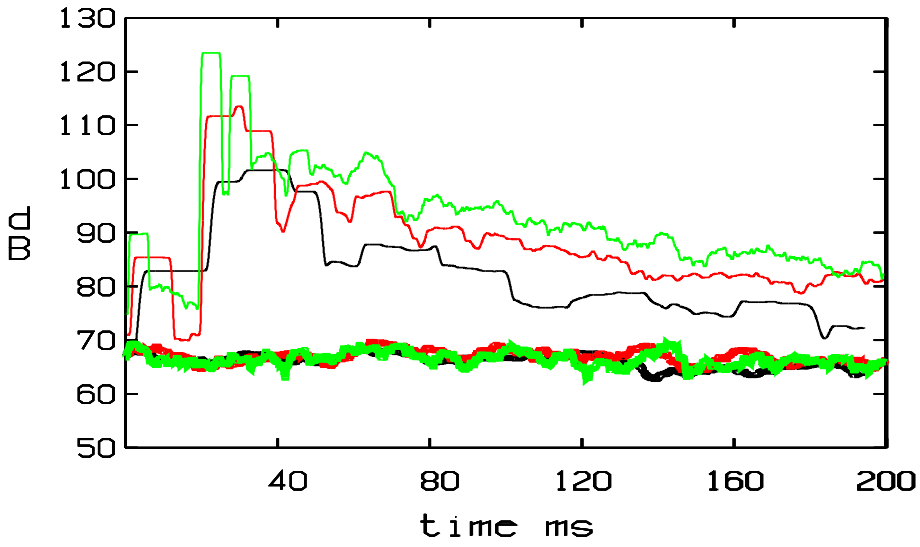

Figure 4.3: *Averaged signal levels in dB re 1 μPa at S04-R2 for $r_c[.5, 60]$ (black), $r_c[1, 30]$ (red), and $r_c[2, 15]$ (green). The corresponding noise levels after stacking and matched-filtering are drawn in thick lines.*

differences in the details, which are hardly significant as the reverberation levels are the same.

It can be seen from Fig. 4.3 that the reverberation still is active at the end of the recording.This also explains why the signal level is higher than the noise floor before the arrival time of the direct wave at 19 ms. The signal has not died out when the recording of the next copy of the stack is started.

The reverberant signal represents an average of the transmission conditions and the scattering strength of the seabed. The statistical basis is large because of accumulation of scattering contributions over a large area as opposed to the head of the signal, which is a single footprint of the sub-bottom below the source.

The strongest arrivals in Fig. 4.1 are the direct and the surface reflected waves. They do not yield information on the geoacoustics of the sediment. Yet they are important for accurate determination of the deployment geometry and the source level.

4.2 The seabed reflection coefficient

The velocity contrast at the seafloor is of crucial importance for long-range propagation in the sea, because it determines the angular range of grazing angles of total relection. Information about the velocity and density at the top of the sediment can be obtained from the initial bottom echo. Fig. 4.4 shows all measured signals at the first receiver R1 in the time-window 4-10 ms around the expected arrival time 6.7 ms of the bottom bounce. Both the source and the receiver are 5 m above the seafloor and the horisontal separation is 2 m. The travel times of the direct and the bottom reflected paths are 5 ms apart, which is long enough to permit a period of silence in between. However, looking at Fig. 4.4, the time span of expected silence (2-6 ms) is occupyied by oscillatory signals of varying amplitudes. The 0.5 kHz Ricker pulse is too corrupted, while the

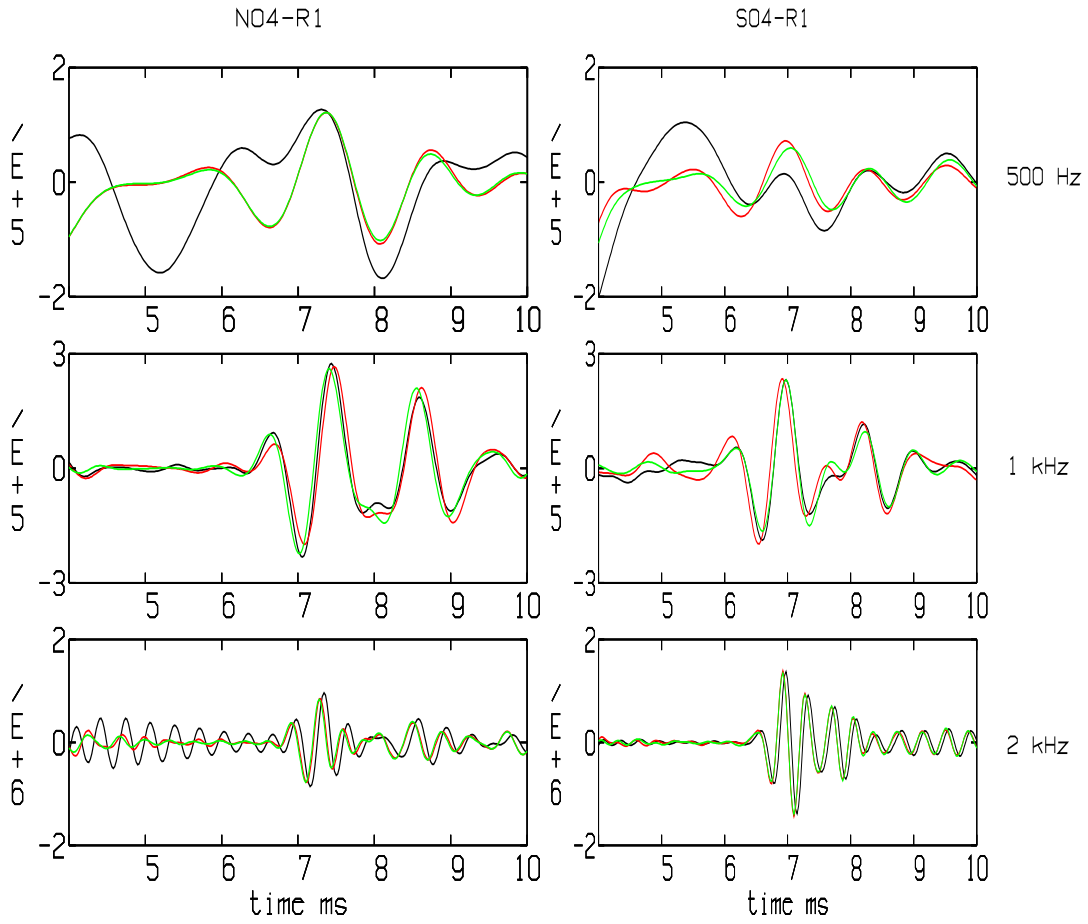

Figure 4.4: *The received signals in a time window around the expected arrival time of the bottom bounce (7 ms). The left panels show the the recordings at N04, the right ones at S04. The pulses centred at .5 , 1 and 2 kHz are displayed from top to bottom with Ricker pulses in black, and short and long Ricker chirps in red and green, respectively.*

1 and 2 kHz pulses are acceptable for a quantitative reflection analysis. It is also seen that the Ricker chirps perform better in suppressing the noise prior to the arrival of the bottom echo.

Next we consider reflection at a horizontal interface between two fluid media with the densities ρ_1, ρ_2 $[g/cm^3]$ and the velocities c_1, c_2 $[m/s]$.The reflection of a spherical wave at a plane surface can approximated by plane wave reflection if the image source is far from the receiver in terms of number of wavelengths [26]. As this condition is only weakly satisfied here, the plane wave analysis should be supported by further evidence. When the angle of incidence of a plane wave travelling from the upper (1) to the lower (2) medium is denoted by θ, the reflection coefficient r is given by

$$r = \frac{Z_2 \cos\theta - Z_1(1 - (\frac{c_2}{c_1})^2 \sin^2\theta)^{\frac{1}{2}}}{Z_2 \cos\theta + Z_1(1 - (\frac{c_2}{c_1})^2 \sin^2\theta)^{\frac{1}{2}}}, \tag{4.1}$$

where

$$Z_1 = \rho_1 c_1 \quad \text{and} \quad Z_2 = \rho_2 c_2,$$

are the characteristic impedances of the media $[gm/cm^3s]$. For medium 1 (seawater) $\rho_1 = 1.0$, while the velocity is set to the measured values at the bottom, that is, $c_1 = 1425$ and $c_1 = 1435$ at N04 and S04, respectively. The square of the reflection coefficient is the relative amount of energy being backreflected. For this reason the reflection coefficient is often referred to as the reflection loss $20log|r|$. This quantity can be obtained from data by a partition of transmission loss into reflection and spreading losses, the latter being known from the geometry. In the present case the angle of incidence is 11°. For angles close to normal incidence, the approximation

$$(1 - (\frac{c_2}{c_1})^2 \sin^2\theta)^{\frac{1}{2}} \approx (1 - \sin^2\theta)^{\frac{1}{2}},$$

is reasonably accurate. Therefore we shall apply the formula

$$r = \cos\theta \frac{Z_2 - Z_1}{Z_2 + Z_1} \tag{4.2}$$

with $\cos\theta \approx 0.98$ for $\theta = 11°$. As r, or equivalently the reflection loss, is obtained from data, the formula (4.2) becomes an equation for the characteristic impedance Z_2 of the topmost part of the sediment. The result of this analysis as applied to data in Fig. 4.4 for the long Ricker chirps is listed in Tab. 4.1

pulse	N04			S04		
	data			data		
	r	$20log\|r\|$	Z_2	r	$20log\|r\|$	Z_2
$Rc[1, 30]$	0.089	21	1710	0.070	23	1650
$Rc[2, 15]$	0.089	21	1710	0.126	18	1860

Table 4.1: *Measured reflection loss and calculated surface impedance.*

Next we examine the reflection coefficients at R2 at the offsets 22.0 and 27.5 m at N04 and S04 respectively. The expected arrival times of the direct and the bottom reflected paths are 15.3 and 16.8 ms at N04 and 18.9 and 20.2 ms at S04. The time separation between the arrivals is too short for a clear identification of the weak bottom bounces except for the 2 kHz pulses. Fig. 4.5 displays the envelopes squared of the long Ricker chirp for the bottom reflections at N04 and S04.

The peak values are 113 and 103 dB, which are 30 dB above the noise floor. The reflection losses are 20 and 28 dB respectively, which are remarkably high in view of the fact that the grazing angles are just 24.5° and 20°. A typical value of a silty sediment is around 12 dB, while sandy sediment would be around 5 dB [27]. By inserting the previous estimates of Z_2 (1710 resp. 1860) into the reflection formula (4.1), it can be solved for c_2 using observed values of r. The resulting velocities are 1423 m/s at N04 and 1394 m/s at S04. In the August 2002 experiment the velocity of the upper part of the sediment at N02 was estimated to 1390 m/s using lateral wave analysis. These results indicate that the surface velocity of the sediment is about the same as the water velocity or even somewhat lower. Using the previous estimates of the impedances we arrive at densities around 1.2 at N04 and 1.3 g/cm^3 at S04.

The lengths of the pulses being used are too large for distinguishing the direct wave from the bottom surface reflection at N04-R3 and S04-R3 at the offsets 58.7 and 48.6

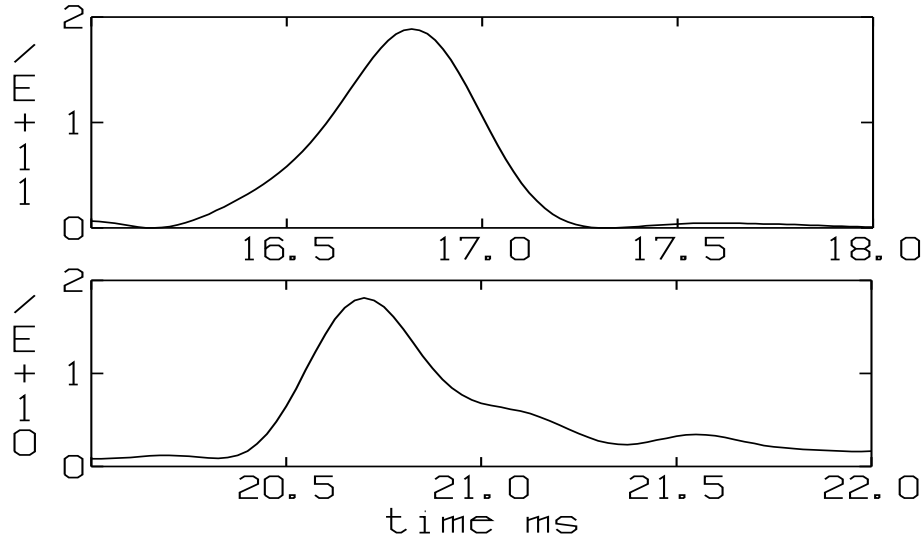

Figure 4.5: *Envelope squared ($[\mu Pa^2]$) of the bottom reflection at N04-R2 (top) and S04-R2 (bottom).*

m. The increased time resolution provided by a 4 kHz pulse would have been beneficial in supplying additional reflection data.

There is only one observation of a bottom reflection from the August 2002 experiment. This measurement was taken at site S02 with the source and a receiver suspended from the support ship (HMS Urd) 4.5 m above the seafloor. The horizontal separation was 10.6 m. The travel distance along the bottom path was 13.9 m and the grazing angle 40°. The expected arrival times of the direct and bottom reflected paths are 7.2 and 9.5 ms. The measured pressure amplitude (uncalibrated) is shown in Fig. 4.6.

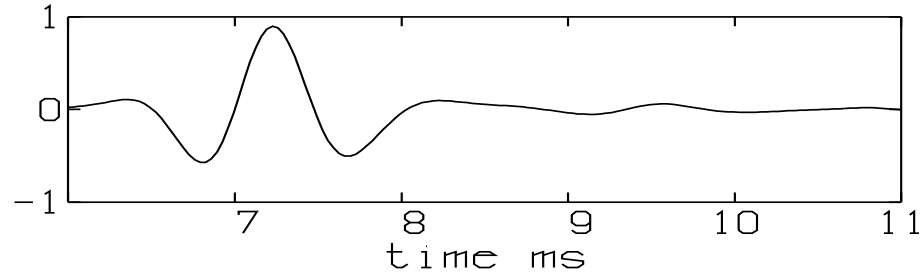

Figure 4.6: *The direct arrival is seen at 7.2 ms and a weak bottom reflection at 9.5 ms. The measurement was taken at S02 for a 750 Hz Ricker pulse. The pressure amplitude is uncalibrated.*

Although there are no calibrations the reflection coefficient can be computed as

$$r = \frac{13.9A_b}{10.6A_d},$$

where A_d and A_b are the uncalibrated amplitudes of the direct and bottom reflected waves. Using numerical values from the recordings, it was found that $r = 0.085$ or a reflection loss of 21 dB. The corresponding loss computed by the formula (4.1) using the values $\rho_2 = 1.3$ and $c_2 = 1400$ previously found at S04 is 20 dB.

The results of the seabed reflection analysis can be summarized as follows. The velocity of the surficial part of the sediment is around 1400 m/s at both sites and the density varies in the range 1.2-1.3 g/cm^3. It implies that the seafloor itself is largely transparent to incident sound waves even at low grazing angles.

4.3 Sub-bottom echoes

The seabed reflection analysis showed that sound directed towards the seafloor propagates further into the seabed. In tracing sound waves in the seabed the presence of sub-bottom echoes is of particular interest. Referring to Fig. 4.1, the strongest arrival at N04 after the direct wave and surface reflection, appear at 31, 37 and 51 ms at R1, R2 and R3 respectively. These echoes may originate from a common reflector beneath the seafloor. They may also be mistaken for returns within the water volume as inshore escarpments or shorelines. Such questions can be resolved by model calculations which could decide whether the arrival times and echo amplitudes are consistent with reflections from the same sub-bottom interface of two different media. Before doing this, further attention must be directed to the information content of measured data of sub-bottom echoes. Fig. 4.7 shows the most distinctive bottom echo at N04 and N02 at all receivers and all signals of interest.

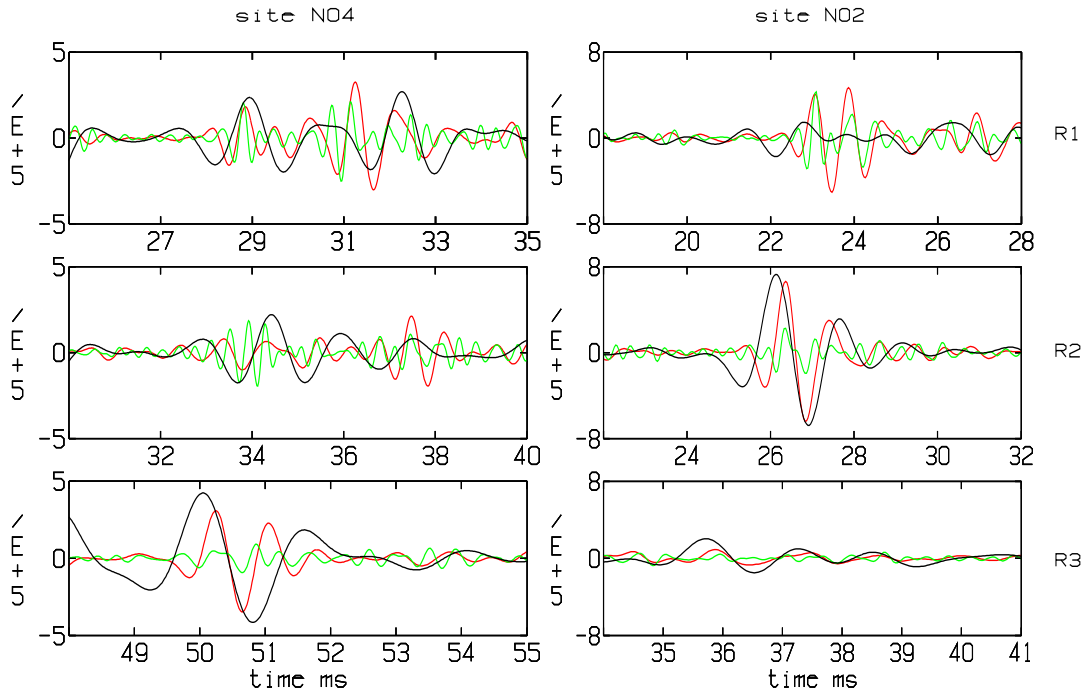

Figure 4.7: *Pressure amplitudes* $[\mu Pa]$ *at the receivers R1, R2, and R3 at the sites N04 (left panels) and N02 (right panels) in time windows corresponding to reflections from a sub-bottom interface some 20 m below the seabottom. The transmitted pulses at N04 are* $r_c[.5, 60]$ *(black),* $r_c[1, 15]$ *(red) and* $r_c[2, 15]$ *(green) and those at N02* $r_a[0.5]$ *(black),* $r_a[1]$ *(red) and* $r_a[2]$ *(green). The received amplitudes have been scaled as if were all transmitted with the power output* 150 *dB.*

These pictures illustrates the principal features of measured data of sub-bottom echoes. As will be evident later by the inversion analysis, the arrival times are all consistent within a few milliseconds with returns from a reflector some 20 m beneath the seafloor. At each receiver the echoes exhibit slighly different arrival times and various pulse shapes depending on the center frequency. Some waveforms correlate well with the transmit pulse, while others are distorted or broken into multiple returns. Despite elongated reflections, the intensity of the strongest echoes is high and the loss is barely more than the spreading loss.

A comparison between the echo levels at N04 and N02 can be made by an inspection of the graphs in Fig. 4.7. Even though the intensity is less at the elevated source-receiver configuration at N04, all echoes possess good SNR.

5 Inversion analysis

5.1 The ray tracing model

Measured data can only be interpreted by comparisons with a physical model. When the predictions made by the model agree with the observations the model may embody new knowledge about the environment. In this study a ray tracing model is used for acoustic wave propagation in the water as well as in the seabed. The environment is assumed to consist of a number of plane-parallel layers. The top layer is the water volume followed by a multilayered seabed in which the last layer is assumed to be a semi-infinite basement of rock. Each layer is characterized by three geoacoustic parameters, speed of sound, density and absorption. In the model these parameters are allowed to vary by depth only.

The ray code RAYLAB [28] was written specifically for tracing sound paths in multilayered media with horizontal stratification. The basic computational unit is the eigenray solver, which computes any ray path between two given source-receiver positions. The tracing may include paths within the sediments. The output is the coordinates of the trace, travel time and transmission loss (TL). Fig. 5.1 and Tab. 5.1 illustrate the main features of RAYLAB.

ray code	time $[ms]$	TL $[dB]$	TL-geo $[dB]$	TL-ref $[dB]$	TL-abs $[dB]$	angle deg
-11	33.53	33.7	33.7	0	0	-2.20
11	34.37	60.1	33.0	27.1	0	10.37
-11	38.31	35.0	35.0	0	0	-29.38
1221	42.74	47.0	36.0	5.9	5.1	38.84
123321	49.15	44.0	38.8	1.3	3.9	53.67

Table 5.1: *The information provided for the ray diagram in Fig. 5.1 includes travel time, TL, losses due to spreading (TL-geo), reflections/refractions (Tl-ref), and absorption (TL-abs). The last column is the angle of departure at the source. The only parameter that depends on the frequency is TL-abs, which depends linearly on the frequency. Here it is given for the frequency 1 kHz.*

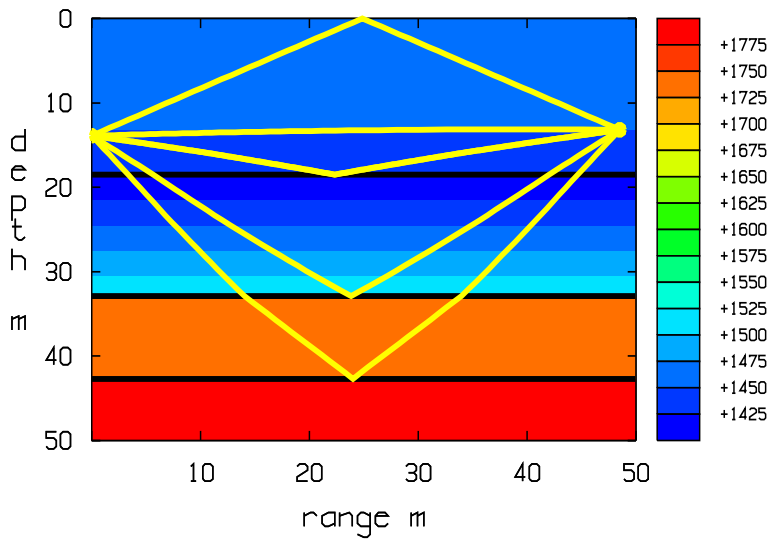

Figure 5.1: *Ray diagram for the deployment geometry at S04-R3 and layer depths as obtained by the inversion of measured data at S04 (see Tab. 5.2). The background is colored according to the velocity profile of the water and the inversion result for the velocity of seabed at S04.*

The first column contains a ray identifier which signifies the layers traversed by the ray. Rays which takes off towards the sea surface are preceded by a minus sign. In the present case the direct ray is slightly curved due to the downbending velocity profile. This ray changes directions by refraction within the water layer and for this reason it has the same notation -11 as the surface reflected ray. The ray 123321 traverses both sediments twice as it is backreflected at the deepest interface. This ray is of particular importance for the inversion analysis because TL along for this path is modest. With reference to Fig. 4.1 it corresponds to the double echo around 50 ms seen in the lower right panel.

Simulations by the ray model can be performed with extraordinary computational speed. The trade-off is a number of simplifying assumptions which could make it inadequate for interpretation of acoustic data. For instance, in a ray model with plane-parallel layers, the arrival time of a sub-bottom echo does not depend on the bandwidth of the pulse. Referring to Fig. 4.7, data exhibits fluctuations both in arrival times and pulse shapes which are not reproduced by the present model. Presumably the variability of measured returns are caused by surface roughness of the reflector on a scale of several meters. The impact of an uncertainty of several milliseconds in using a plane-layered model depends on the source-receiver configuration. For a close-range receiver a time spread of that order is acceptable for the determination of a layer depth around 20 m as the uncertainty is limited to a few meters. The sensitivity issue is reversed for velocity estimates based on travel times. Then the adverse effect of time uncertainty decreases at larger source-receiver offsets [17]. Therefore reasonable accuracy is achievable if there are receivers with well-balanced separations.

The assumption that the seabed behaves like a fluid medium from an acoustical point of view may be questioned. Notwithstanding inversion attempts are beneficial as they

may pinpoint the shortcomings of the model and pave the way for model improvements.

5.2 The inversion scheme

The inversion scheme consists of two parts in which layer velocities (c) and thicknesses (h) are determined independently of layer densities (ρ) and absorption values (α).

The inversion for c and h is done one layer at a time starting at the top layer. In case the velocity is assumed to be uniform there are two target parameters of each layer. The velocity may also be sought as a depth profile with a number of shape parameters which should be less than the number of receivers to avoid ambiguous estimates. The inversion for c and h is based on a matching of measured and computed travel times at all receivers. A best fit is obtained by minimizing the fitness function

$$F = \left(\frac{1}{M} \sum_{m=1}^{M} (t_m^{dat} - t_m^{ray})^2 \right)^{\frac{1}{2}}, \tag{5.1}$$

where

$$\begin{aligned} \text{M} &= \text{number of receivers} \\ t_m^{dat} &= \text{measured travel time at the mth receiver} \\ t_m^{ray} &= \text{computed travel time at the mth receiver} \end{aligned}$$

Here t_m^{ray} is obtained by computing the travel time along an eigenray path from the source via a path through the seabed to the target sediment layer, where it is traced back to the receiver after reflection at the bottom of the layer. For each choice of c and h within the search space of the fitness function, such a tracing is required for all receivers. Once c and h of the top layer have been determined they are inserted into the geoacoustic model, which makes it possible to compute travel times for paths in the underlying layer. The top-down approach of performing a sequence of optimization problems with merely two target parameters is cost effective compared to a single inversion for the entire layer configuration.

The difficulty is to extract travel times t_m^{dat} from the measured time-series of pressure. Assume an inversion is to be made for N layers. The N observations of t_m^{dat} are required at each receiver corresponding to reflections from a sequence of N layer interfaces at increasing depths. The time-ordered sequence of t_m^{dat} at each receiver must correspond to echoes from the same layer interfaces. A mismatch of echo times would make the fitness function F to depart from the ideal value $F = 0$.

The extraction of t_m^{dat} from measured data is organized as follows by the inversion software. At N04 and S04 the long matched-filtered Ricker chirps are used as input data, while Ricker pulses are used at N02 and S02. There are three time traces at each receiver for pulses with the bands 0.5, 1 and 2 kHz. Identification of echoes is applied to the envelope squared in a time-window with gaps for known arrival times along ray paths entirely confined to the water. An echo is defined as a local maximum of the envelope squared and the strength is the minus of TL measured with respect to the peak value. The echoes are searched in decreasing order of strength and put into bins placed on the time axis with a width of 4 ms. The bins are common for all

pulses but only the strongest echo from each pulse is saved. Thus there are at most one echo from each pulse within a single bin, which now is ascribed a strength equal to the sum of energies of its echoes. When the screening for echoes is completed the bins with the N largest energies at each receiver are marked for an N-layer inversion. If a bin contains several echoes the one with the smallest TL is being used for t_m^{dat} of the inversion scheme. This implies that for each of the layers the pulse with the strongest echo is selected for each receiver.

The inversion for layer densities (d) and absorption parameters (α) are based on measured TL of the same echoes as being used for the inversion of c and h. In the ray model TL can be separated into losses due to geometrical spread, absorption and reflection/transmission at layer interfaces. The latter loss depends on the geoacoustic parameters on both sides of a media interface. This coupling implies that the inversion comprises a $2N$-dimensional search space of the target parameters d and α for all layers. The fitness function D for this problem is formulated as

$$D = \left(\frac{1}{MN} \sum_{n=1}^{N} \sum_{m=1}^{M} (TL_{mn}^{dat} - TL_{mn}^{ray})^2 \right)^{\frac{1}{2}}, \tag{5.2}$$

where

$$\begin{aligned} \text{M} &= \text{number of receivers} \\ \text{N} &= \text{number of layers} \\ TL_{mn}^{dat} &= \text{measured TL in dB at the mth receiver of the nth echo} \\ TL_{mn}^{ray} &= \text{computed TL in dB at the mth receiver of the nth echo.} \end{aligned}$$

The computation of TL_{mn}^{ray} takes only a few arithmetic operations when the corresponding eigenray has been found. The computations the eigenrays can be done in advance using the inversion results for c and h.

5.3 Inversion results

The number of layers and the format of the depth dependence of the target parameters of each layer must be set by the user prior to the inversion. In future this task should be computerized as it requires analysis of data with respect to the presence of useful echoes at different receivers. Based on echo analysis of the type presented in Sec. 4.3, a 2-layer inversion seemed to be appropiate in the present case. On the basis of the seabed reflection analysis in Sec. 4.2, the velocity of the top sediment at the water-sediment surface was fixed to 1400 m/s. For the same reason the density at the seafloor was set to 1.2 g/cm^3 at N02 and N04, and 1.3 g/cm^3 at S02 and S04. Instead c and d were assumed to increase linearly by depth of the top layer. This was accomplished by defining c and d as target parameters at the bottom of the top layer (denoted by c_{bot}, d_{bot}). The absorption of both layers and c, d of the second layer were each represented by a single target parameter, that is, they were not allowed to vary by depth. The best fit was found by an exhaustive search as the target parameters were varied according to Tab. 5.2.

target parameter	layer no	initial value	final value	step size
h $[m]$	1	1	30	0.1
h $[m]$	2	1	30	0.1
c_{bot} $[m/s]$	1	1400	2300	10
c $[m/s]$	2	1400	3000	25
ρ_{bot} $[g/cm^3]$	1	1.2 (1.3)	2.3	0.05
ρ $[g/cm^3]$	2	1.2 (1.3)	2.3	0.05
α $[dB/\lambda]$	1	0	0.5	0.01
α $[dB/\lambda]$	2	0	0.5	0.01

Table 5.2: *The discrete search space of target parameters.*

The results of the inversions are presented in Tab. 5.3. The preset values of c and d at the water-sediment surface have been included for completeness in both Tab. 5.2 and 5.3.

test site	layer no	h $[m]$	c $[m/s]$		ρ $[g/cm^3]$		α $[dB/\lambda]$	fitness	
			top	bottom	top	bottom		F $[ms]$	D $[dB]$
N02	1	6.2	1400	1400	1.2	1.2	0.42	0.51	2.5
N02	2	10.6	1650	1650	1.7	1.7	0	0.23	2.5
N04	1	4.8	1400	1400	1.2	1.3	0.43	0.88	3.2
N04	2	13.7	1550	1550	1.5	1.5	0	0.21	3.2
S04	1	14.4	1400	1520	1.3	1.3	0.16	0.18	1.6
S04	2	9.8	1746	1746	2.1	2.1	0	0.75	1.6
S02	1	15.2	1400	1490	1.3	1.3	0.13	0.01	4.0
S02	2	9.8	1490	1490	1.8	1.8	0	0.13	4.0

Table 5.3: *The inversion results at all sites.*

The computational load for each inversion was some $1.5 \cdot 10^5$ evaluations of t_m^{ray} and $4.3 \cdot 10^6$ of TL_{mn}^{ray}, which were executed within a time span of 10 s.

The values of the fitness functions (5.1) and (5.2) are listed at the right end of Tab. 5.3. The F values at S02 are exceptionally small because data only at two receivers were available at S02. It implies that there are two unknowns (c and h) and two constraints for the geometry of each layer. The solution to this system, if any, would make $F = 0$. However in cases with uncertainties it is preferable to oversupply data because a mismatch of echo time data at the receivers would affect F adversely. Even though the excess of data with three receivers is small, the obtained values of F in Tab. 5.2 are reasonably small. Fig. 5.2 is a level plot of the fitness function F of the inversion for c and h of the second sediment layer at N04. The minimum is located in a valley with an elongation that reflects the difficulty of resolving the velocity-thickness ambiguity.

The vanishing of the absorption parameter of the bottom layer at all sites reveals a deficiency of the inversion algorithm related to the selection of echoes. For a given receiver and layer only the strongest echo is submitted to the inversion scheme. For

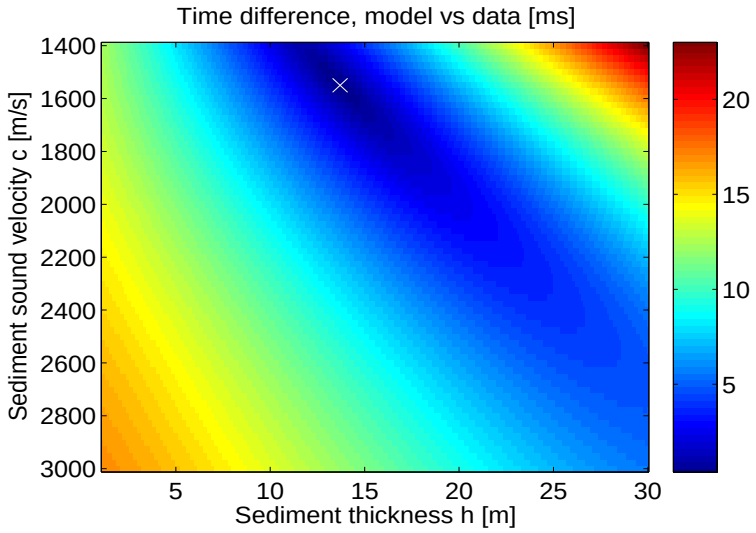

Figure 5.2: *The fitness function (5.1) in ms for the rms deviation between measured and computed travel times of sound waves reflected at the bottom of the second layer. The best fit for $h = 13.7$ m and $c = 1550$ m/s is marked by a cross.*

the bottom layer it turns out that the 0.5 kHz pulse is the preferred choice, while pulses with larger bandwidths were selected for inversion of the top layer. The attenuation of the bottom layer at N02 was found to be 0.1 dB/λ in [17] by observing the absorption loss of the 2 kHz pulse. Assuming such a small loss value, the expected absorption loss at 0.5 kHz for a two-way path to the bottom of the second layer would be 0.5-1.5 dB depending on the offset of the receiver. Apparently this loss was not discernable as it is within the uncertainty of the measured echo level.

For comparison the inversion result at N02 as reported in [17] is shown in Tab. 5.4. It was obtained in a hand-made fashion along the same lines as now have been automatized.

test site	layer no	h $[m]$	c $[m/s]$		ρ $[g/cm^3]$		α
			top	bottom	top	bottom	$[dB/\lambda]$
N02	1	6.6	1425	1425	1.5	1.5	0.15
N02	2	10.7	1664	1664	1.7	1.7	0.1

Table 5.4: *The inversion result from [17] at N02.*

Comparing the inversion results at the co-located sites N02 and N04, the most noticeable difference is the velocity estimates 1650 respectively 1550 of the deep layer. Otherwise the overall agreement is good in view of modeling and measurement uncertainties. The observation indicates that the inversion works even for elevated sensor positions at some height above the seafloor.

Comparing the results at N04 and S04 it is observed that the depth to the deep reflector increases by 7-8 m at S04. The large difference of the thicknesses of the top layer is of less importance as the reflections from the intermediate interface are much weaker than those from the bottom of the deep layer.

6 Conclusions

Although there are reservations concerning the use of a plane-parallel layer model and the weak statistical basis of the data, a unified picture of the overall features of the sediment cover can be summarized as follows:

- the reflection coefficient at the seafloor is very small (< 0.1)
- the velocity and density of the surficial part of the sediment is around 1400 m/s and 1.2-1.3 g/cm^3
- there is a strong reflector at the depth 17-25 m, presumably a rock basement
- the absorption coefficent is of the order 0.1-0.2 dB/λ
- the diffuse scattering from the seabed is large

The following conclusions can be drawn in comparing the sea trials in August 2002 and May 2004 with the source and the receivers on and above the bottom respectively.

- the reflections from the strong reflector within the seabed were weaker by at most 10 dB for the elevated positons, see Fig. 4.7
- the inversion results of the two cases were similar
- a definite advantage of the elevated positions was the measurements of the reflection coefficient of the seafloor

7 Future work

The usefulness of the seafloor reflection coefficient was not foreseen at the planning stage of this experiment. In future the deployment geometry and emitted waveforms should be chosen to improve the quality and the amount of reflection data for direct bottom bounces. In order to resolve the velocity-density ambiguity the measurements must be taken both at near normal incidence and at offsets for which the grazing angles are somewhat larger but close to the critical angle of total reflection. As the critical angle is not known in advance, the offsets must be adapted to varying bottom conditions. Such a flexibility can be achieved by the use of tow-fishes.

The reflection coefficient becomes more important when the impedance of the surficial sediment increases, while the effects of deep seabed returns diminishes. Therefore the seabed reflection coefficient is a prime target parameter for hard sediments and it should be incorporated into the inversion scheme.

Measurements of the seabed reflection coefficient at high frequencies using the amplitude of the direct bottom bounce are common practice since long. The results are often inclusive depending on a number of uncertainties related to the calibration of the source and the deployment geometry. Another difficulty is that the estimates fluctuate by the frequency because of a random variability of the surface layer of the bottom.

Similar perturburations occur if the location of the footprint on the seafloor varies by the angle of incidence of the probing signal. Suggestions how to to deal with these difficulties can be found in [27].

The inversion analysis in this paper is based an geoacoustic model with flat and homogeneous fluid layers. This may be acceptable as a first approximation. Data indicates that sedimentary interfaces are rough on scales of several meters. A starting point on finding the origin of the strong seabed scattering is to inspect the signals for scattering features. Comparisons with reflection data from other types of sediments are helpful in this respect. An efficient way to enlarge the empirical basis is to collect data from mobile platforms.

Reverberation is a major problem of detection performance of active sonars. Reverberation involves two-way sound propagation and scattering from the sea surface, volume and bottom. At low frequencies reverberation data provide a significant amount of information of the average properties of the sea bottom. An advantage of using reverberation for inversion is that data can be obtained from a single platform with a transmitter and a receiver [29],[30]. The benefit of using both reverberation and short range reflection data in geoacoustic inversions is a topic for future research.

Acknowledgement

We thank Ulf Skotte for patience and professional assistance during the field trial.

Stefan Ban made thorough calibrations of the hydrophones both prior to and after the field trial. These measurements are presented in a separate document.

References

[1] J. Pihl, P. Söderberg, A. Wester, and V. Westerlin. A Method for On-site Determination of Geoacoustic Parameters. Methodology report FOA-R-99-01281-409-SE, 1999.

[2] B.L. Andersson and I. Karasalo. Range-dependent seabed parameter inversion with JEPE-S and a genetic algorithm. In *Proc. 5th Eur. Conf. Underwater Acoustics, ECUA 2000*, pages 215–220. Lyon, France, 2000.

[3] L.Abrahamsson and B.L. Andersson. Identification of seabed geoacoustic parameters from transmission loss data. Methodology report FOA-R-00-01752-409–SE, 2000.

[4] L. Abrahamsson and B.L. Andersson. Inversion of seabed parameters in the Stockholm archipelago. Methodology report FOI-R–0300–SE, 2001.

[5] P. Krylstedt and J. Mattson. Numerical modeling of electromagnetic frequency sounding in marine environments: A comparison of local optimisation techniques. In *Proc. 3rd Int. Conf. in Mar. Elec. MARELEC 2001.* Stockholm, Sweden, 2001.

[6] P. Krylstedt and J. Mattson. Environment assessment for underwater electric sensors. In *UDT Europe*. Malmö, Sweden, 2003.

[7] D. Berg, L. Abrahamsson, L. Crona, and P. Sigray. Determination of seabed conductivity by transient VLF sounding. In *Proc. 4th Int. Conf. in Mar. Elec. MARELEC 2004*. London, UK, 2004.

[8] B.L. Andersson and I. Karasalo. LOW-FREQUENCY INVERSION OF SEABED PARAMETERS IN THE BALTIC. In *Proc. 7th Eur. Conf. Underwater Acoustics, ECUA 2004*, pages 671–676. Delft, The Netherlands, 2004.

[9] A. Elhammer, S. Axberg, and B. Kjellin. The Marine Geological Map 079/470, Fårö, Sver. geol. unders. Serie Am 2, 1988.

[10] E. Dalberg, M. Levonen, B. Nilsson, M. Olsson, J. Pihl, and P. Söderberg. Geoacoustic Sediment Properties in the Baltic. Methodology report FOA-R-00-01466-409–SE, 2000.

[11] Studie MTK03163S. Behovet av produktion av sjögeografisk information, 2004.

[12] B.L. Andersson and P. Morén. Studie av geoakustiska data för sonartaktiskt beslutsstödsystem, UwEM och HAIS-III. Teknisk rapport FOI-R–0448–SE, 2002.

[13] P. Kearey, M. Brooks, and I. Hill. *An Introduction to Geophysical Exploration.* Blackwell, 2002.

[14] C. Park, W. Seong, P. Gerstoft, and M. Siderius. Time-Domain Geoacoustic Inversion of High- Frequency Chirp Signal From a Simple Towed System. *IEEE J. Oceanic Eng.*, 28:468–478, 2003.

[15] C.W. Holland and J. Osler. High-resolution geoacoustic inversion in shallow water: A joint time- and frequency-domain technique. *J. Acoust. Soc. Amer.*, 107:1263–1279, 2002.

[16] L. Abrahamsson. An assessment of broadband acoustic techniques for determination of sediment parameters. Methodology report FOI-R–1194–SE, 2004.

[17] L. Abrahamsson, B.L. Andersson, I. Karasalo, and P. Sigray. Environment assessment for underwater sensors in the Stockholm archipelago, part 1 - inversion of hydroacoustic sub-bottom parameters. User report FOI-R–0706–SE, 2002.

[18] N.H. Ricker. *Transient waves in visco-elastic media.* Elsevier North-Holland, 1977.

[19] N. Levanon. *Radar Principles.* J. Wiley, 1988.

[20] R.O. Nielsen. *Sonar Signal Processing.* Artech House, 1991.

[21] S. Ivansson, M. Levonen, and P. Söderberg. Quantitative Determination of Sediment Properties in the Baltic Using Close-Range Seismic Reflection Data. Methodology report FOA-R-00-01555-409–SE, 2000.

[22] B. Berntsen, I. Karasalo, M. Levonen, P. Morén, and V. Westerlin. Seabed characterization in the Baltic with the SIROB and FARIM methods. Methodology report FOA-R-99-01237-409-SE, 1999.

[23] E. Dalberg, L. Frenje, S. Ivansson, and B. Nilsson. Measurements and Modelling of Shallow Water Reverberation. Methodology report FOA-R–00-01751-409–SE, 2000.

[24] M. Levonen, S. Ivansson, P. Morén, and P. Söderberg. Bottom Scattering in Shallow Water Measurements with a Parametric Sonar. Methodology report FOA-R–99-01359-409–SE, 1999.

[25] J. Pihl, L. Abrahamsson, S. Ivansson, and J. Schön. Mid Frequency Bottom-Interacting Sound Propagation and Reverberation in the Baltic. Submitted to IEEE J. Oceanic Eng., 2004.

[26] L. Brekhovskikh and Yu. Lysanov. *Fundamentals of Ocean Acoustics*. Springer-Verlag, 1982.

[27] C.W. Holland. Seabed reflection measurement uncertainty. *J. Acoust. Soc. Amer.*, 114:1861–1873, 2003.

[28] L. Abrahamsson, D. Berg, L. Crona, and P. Sigray. Determination of seabed conductivity by transient VLF sounding. in preparation, 2003.

[29] J-X Zhou, X-Z Zhang, P.H. Rogers, J.A. Simmen, P.H. Dahl, G. Jin, and Z. Peng. Reverberation Vertical Coherence and Sea-Bottom Geoacoustic Inversion in Shallow Water. *IEEE J. Oceanic Eng.*, 29:988–999, 2004.

[30] S.H.E. Muller, M.A. Ainslie, W. Boek, and D.G. Simons. Inversion for bottom parameters using low frequency reverberation data. In *Proc. 6th Eur. Conf. Underwater Acoustics, ECUA 2002*, pages 147–152. Gdansk, Poland, 2002.